UNDERSTAND PROGRESSING CAVITY PUMPS CHARACTERISTICS AND AVOID ABRASIVE WEAR

by

Gerhard Vetter

Professor

and

Wolfgang Wirth

Research Engineer

University of Erlangen-Nuremberg

Erlangen, Germany

Gerhard Vetter obtained his Dipl. Ing. degree (Mechanical Engineering) at Technische Universität Karlsruhe, Germany. After some years as a Research Engineer in turbomachinery at the same university, he joined Lewa, Leonberg (Germany) as head of the Research and Development Department. He became Chief Engineer and, in 1970, Technical Managing Director. In 1981, he accepted a chair (professorship) for Apparatus and Chemical Machinery at the University of Erlangen-Nuremberg.

Dr. Vetter has dedicated more than 25 years to research, development and design of pumps and metering equipment. He has been one of the pioneers in diaphragm pumps development. His many papers, patents and contributions to textbooks have established his reputation as a pump specialist.

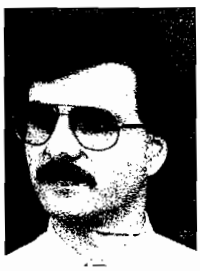

Wolfgang Wirth obtained his Dipl.-Ing. degree (Chemical Engineering) at the University of Erlangen-Nuremberg, Germany (1986) and subsequently joined the Institute of Apparatus and Chemical Machinery at the same institution. As a research engineer, he prepared a thesis about methods for modelling the hydraulic and tribologic properties of progressing cavity pumps and received his Dr.-Ing. degree (1993).

ABSTRACT

Progressing cavity pumps develop their pumping action by the meshing of the external threads of the elastomer stator and the internal threads of the metallic rotor. The special geometry, as characterized by the different pitches of stator and rotor threads and the eccentric motion of the rotor, is creating the displacement chambers, which are periodically discharging by superposition, a constant flow against the pressure differential.

The authors report on the influencing parameters on pump performance with respect to flow-speed-characteristics, volumetric and energetic efficiency and starting torque. In all cases, the rotor/stator overlapping is featuring remarkable influences. Clearances between stator and rotor increase the internal leakages and decrease mechanical friction. Overlapping rotor/stator design yields internally tight pumps, but increased mechanical friction. With theoretical and experimental investigations, an understanding of the pump performance is presented. The tests clearly show an optimum of energetic efficiency to exist for a certain overlapping factor. The theoretical modelling of the pump performance proves to be very difficult, due to tolerances on clearance dimensions from manufacture and thermal or chemophysical expansion as well. But nevertheless, a first rule of thumb for estimating pump efficiency based on leakflow tests and determination of the friction coefficient μ by means of a tribometer are given. Furthermore, hydroabrasive wear tests and possibilities of theoretical modelling are given.

As progressing cavity pumps are frequently used for such applications as transporting abrasive suspensions and slurries, this subject is very important and implementing a new scientific approach. The tribological system in the pump in that service is dominated by sliding hydroabrasive wear. The wear mechanisms is explained and a model presented by considering the intermeshing geometry and the relative time interval for contact of a stator surface element. Field tests with progressing cavity pumps using quartz-suspensions and different material selection demonstrate basically good correlation with the model, indicating clearly that the wear rate varies strongly with the local position on the rotor surface. A large number of tribological tests conducted with a special rotary sliding tribometer that is simulating the rotating and oscillating motion in the progressing cavity pump quite closely, delivered wear rates correlating quantitatively with field test results and, thus, offer a rough possibility for endurance prediction. Based on tribological tests with the adequate tribometer and the real pumping fluid, the optimum pump design may be elaborated.

INTRODUCTION

Progressing cavity pumps are capable of handling a wide spectrum of fluids. The range of applications extends from pumping water out of deep wells [1, 2] to the transport of highly viscous fluids intermixed with particles, even to pumping of ready-mixed stucco and plaster at construction sites (Figure 1). For an economical employment of these pumps, it is essential to understand the different potential influences on the transport capacity, the efficiencies and the service life of the pump.

The pump is characterized by the following favorable features:

- typical pump for low flow/high head conditions.
- single screw pumps are distinguished by an almost nonpulsating discharge
- sliding internal sealing line.
- clearance between the transport elements quasi elastic -> qualified for the transport of abrasive fluids.

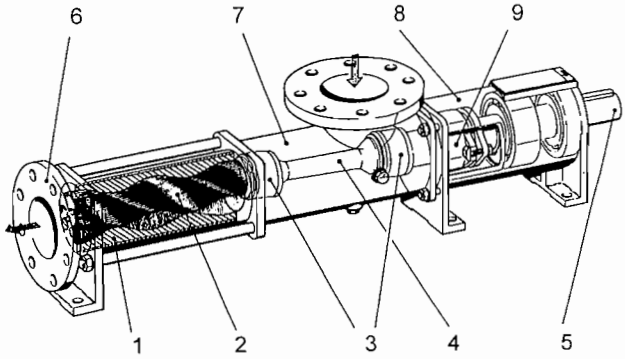

Figure 1. Design of a Modern Progressing Cavity Pump [3]. 1) stator; 2) rotor; 3) cardan coupling; 4) cardan shaft; 5) drive shaft; 6) discharge flange; 7) pump housing; 8) bearing housing; and 9) seal housing.

- tribological system: metal/elastomer.

The progressing cavity pump delivers against pressure differentials up to six bar (single stage design) and up to 72 bar (12 stage design). The pump can be run within systems operating at pressure levels of maximum 160 bar. The pump is selfpriming for suction conditions up to approximately 9.0 m suction head. The discharge flow ranges from 10 l/h to 600 m^3/h at drive speeds between 30 and 3000 rpm. Large pumps may need 100 kW of drive power. Fluids with a viscosity between 1 and 1,000,000 mPas, even containing considerable amounts of solids, can be handled. Temperatures between -40°C and 300°C are acceptable, the limits depending on the properties of the material used for the stator. Using highly chemically resistant types of elastomers for the stator the pump shows extended service life handling even corrosive fluids.

The pump for a certain case of application is characterized by the pump geometry, the materials involved, the fluid to be transported and the operating point on the characteristic.

The authors' intent is to provide an understanding about the influences on the hydraulics and the power requirements of the pump. Additionally, a procedure for a wear prognosis and lifetime estimation based on tribometric tests will be presented.

Contrasting with centrifugal pumps, the transport of fluid does not rely on hydrodynamic effects, but is accomplished by hydrostatic displacement of defined volumes of fluid. Accordingly, the pump achieves significantly higher delivery pressures. The economical volume flow is, however, substantially lower than in centrifugal pumps. The discharge flow is largely independent of the head, a typical feature of the pump. The characteristic is stiff with respect to the head. Consequently, the pump is able to transport fluid across the entire range of the rotational speed.

Principal Designs

In most cases, the rotor is driven via a cardan coupling. Depending on the head, single, and multiple stage pumps are built. In addition to the horizontal arrangement of pump and motor, vertical features, sometimes with submergible motors, are possible. For exceptionally high viscosity, a feeding helix preceding the pump is necessary to improve the $NPSH_r$. The housing will then show an especially large rectangular feeding cross section.

Media unable to flow as, e.g., nearly dry substances from filter presses or decanters, require in addition to the feeding helix, stuffing paddles in the feed cross section to avoid bridging.

In the food industry, the pump is employed in a configuration allowing rapid cleaning. Such pumps are characterized by streamlined design without dead ends or inaccessible pockets to eliminate hiding places for bacteria. They can be disassembled without requiring special tools. Special designs within this concept are cleaning in place pumps (CIP-pumps) and pumps that can be sterilized for the use in biotechnology or in the pharmaceutical industry (SIP = sterilizing in place).

Elements of the Pump

Rotor/Stator Design

Usually a hard rotor operates against a soft elastomer stator. In a new pump, some positive overlapping (i.e., rotor larger than stator) exists between these transport elements to assure good hydraulic efficiency.

For high pressure differences multistage configurations are used. In exceptional cases, up to 12 stages are employed in a pump. As a general rule, each stage is able to handle approximately six bar pressure difference.

The pump is normally equipped with a solid elastomer stator offering a large elastic volume for deformations. The adjustable stator (Figure 2 (a) and (b)) allows by tightening correction of the wear and reduction of slip.

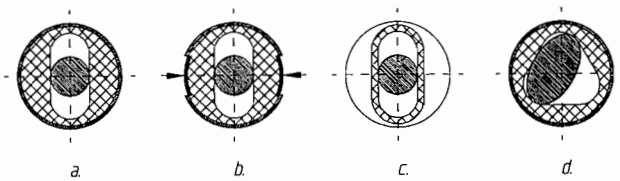

Figure 2. Pump Stators. (a) (b) adjustable stator [4]; (c) stator with uniform wall thickness [6]; and d) special inner contour of the stator with three helices instead of two [4].

The stator with uniform wall thickness (Figure 2 (c)) has less elastomer volume subject to filling and, therefore, yields lower losses due to friction.

At the same time, the stability of the shape is better than in solid stators. The admissible pressure per stage can be doubled (12 bar). Additionally, the lower thickness of the wall permits higher manufacturing precision and, therefore, more precise adjustment of the amount of overlapping (i.e., clearance). As a result, the startup momentum and the wear are reduced.

Rotors are manufactured in a solid and hollow designs. Hollow rotors exhibit lower centrifugal forces. They are particularly used in large size pumps and cause a favorable substantial increase in the service life of the transport elements.

Multiple thread geometries (Figure 2 (d)) feature larger transport chambers. The rotational speed can be lowered and higher pressure differences per stage are feasible thanks to the higher stiffness of the elastomer stator.

Cardan Couplings

The original pinjoint is still used as a simple, inexpensive variety. The dominating design actually is the cardan geared coupling with curved teeth. For special applications, a multitude of customized designs are available (e.g., for quick cleaning, with special seals).

In rare cases, elastic drive shafts without joints are seen. This design requires a larger distance between motor and rotor and exerts additional transverse forces.

PUMP CHARACTERISTICS

Following an introductory review of the basic principles of the pump, the pump performance with respect to the discharge

flow, the power consumption, efficiencies and the parameters influencing these characteristics will be explained.

Discharge Principle and Energy Balance

The displacement is based on the interaction of the eccentrically rotating rotor and the fixed stator, which are characterized by the geometrical dimensions (Figure 3).

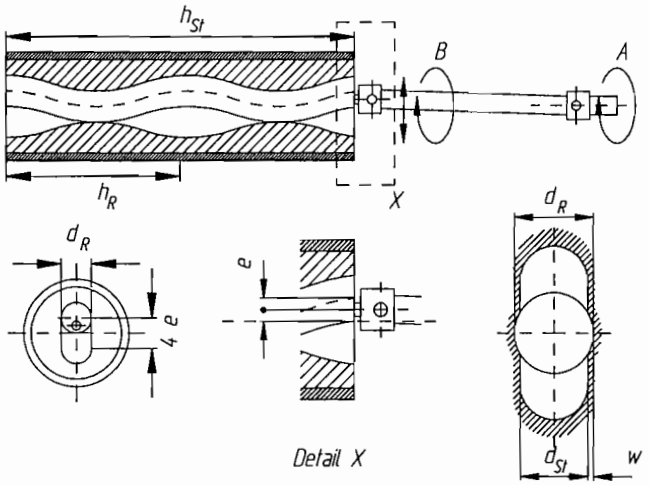

Figure 3. Geometry of the Displacement Elements.

The clearance, i.e., overlapping between the rotor and the stator is defined as:

$$w = \frac{d_R - d_{St}}{2} \tag{1}$$

Clearance ($w < 0$) describes combinations of the displacing elements with inner gaps between the elements along the sealing lines, positive overlapping ($w > 0$) results in clamping between the transport elements along the sealing lines.

The displacement geometry is defined by the shape of the stator and the rotor. The rotor constitutes some kind of a screw with rounded threads, extremely steep pitch and a small core diameter. The stator serves as a "nut" for the screw with twice the pitch as the rotor.

By this configuration, transport volumes, moving towards the discharge side of the pump during rotation of the rotor, are maintained between the rotor and the stator.

At any arbitrary cross section of the transport elements, the rotor and the stator contact each other at two opposite points. Two longitudinal sealing lines delimitating the transport chambers along the pump form the connection between all these sealing points in the axial direction.

Delimitating of the faces of the transport chambers takes place by semicircular sealing lines at the top dead position of the rotor, i.e., in the places where the rotor is flush with the semicircular contour of the stator cross section.

The course of the longitudinal sealing lines and the position of the facial sealing lines changes continuously with the progress of the rotational angle, φ, of the rotor. Projections are shown in Figure 4 for an arbitrarily picked angular position of the longitudinal sealing lines on the cross sections of the transport elements. The length of the sealing lines can be computed from the geometrical data of the pump.

For zero clearance between the transport elements, the geometrically determined volume flow, Q_{th}, can be expressed as:

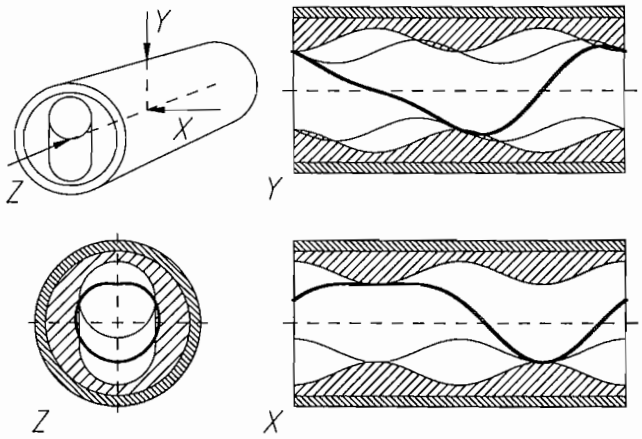

Figure 4. Sealing Lines.

$$Q_{th} = D \cdot n = 4 \cdot d_R \cdot e \cdot h_{St} \cdot n \tag{2}$$

Usually the transport elements are designed with overlapping ($w > 0$); the diameter of the rotor is then slightly larger than the diameter of the width of the stator (typically $d_R/d_{St} \approx 1.01$).

The geometrically determined transport flow Q_{th} for pumps with internal clearances, where the rotor diameter is slightly smaller than the width of the stator ($w < 0$), shows the following relation to the clearance w:

$$Q_{th} = \left[4 \cdot e \cdot d_R - 8 \cdot e \cdot w - \pi \cdot (d_R \cdot w + w^2)\right] \cdot h_{St} \cdot n \tag{3}$$

For pumps with overlapping between the displacement elements, the transport flow can be described by the following expression [6]:

$$Q_{th} = \left\{ 4 \cdot e \cdot d_R - 8 \cdot e \cdot w - \pi \cdot (d_R \cdot w - w^2) + 2 \cdot \left[\frac{\pi}{4} \cdot \arcsin \left(\frac{2 \cdot \sqrt{d_R \cdot w - w^2}}{d_R} \right) - \sqrt{d_R \cdot w - w^2} \cdot \left(\frac{d_R}{2} - w \right) \right] \right\} \cdot h_{St} \cdot n \tag{4}$$

This characteristic shows the decrease of the geometrically determined volume flow as the overlapping increases. The flow of energy and fluid in the pump can generally be illustrated by means of Figure 5.

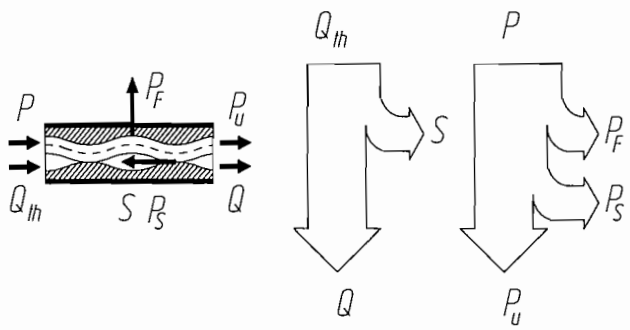

Figure 5. Flow and Power Consumption of the Positive Displacement Pump.

The pump delivers not the entire geometrically determined volume flow, Q_{th}, since part of it flows back to the suction side as internal slip, S. The power, P, entered into the pump is partly delivered as effective power, P_u, the remaining parts are the losses due to friction, (P_F), and slip, (P_S).

Discharge Flow

The effective discharge flow, Q, represents the difference between the geometrical discharge flow, Q_{th}, and the internal slip, S.

$$Q = Q_{th} - S = D \cdot n \cdot \eta_v = Q_{th} \cdot \eta_v \tag{5}$$

The theoretical volume flow is determined by the entire geometry of the pump and by the operational speed of the drive.

$$Q_{th} = f\,(d_R, e, h_{St}, w, n) \tag{6}$$

The volumetric efficiency η_v is influenced by the internal slip of the pump,

$$\eta_v = \frac{Q}{Q_{th}} = \frac{Q_{th} - S}{Q_{th}} \tag{7}$$

The slip S in turn depends on the pressure difference across the pump, the geometry of the clearances and the viscosity of the fluid:

$$S = f\,(\Delta p, \eta, s) \tag{8}$$

For laminar and turbulent flow through the clearances, the slip flow can be roughly expressed as:

$$\text{laminar: } S_{lam} \sim \frac{\Delta p \cdot s^3}{\eta} \qquad \text{turbulent: } S_{turb} \sim \sqrt{\Delta p \cdot s^3} \tag{9}$$

These Equations (9) yield the basic characteristics for the volume flow for pumps with overlapping (w > 0) or clearance (w < 0).

The characteristics of pumps with clearance (Figure 6 (a) and (c)) are influenced by the internal slip, S, which, according to Equation (9), depends on the pressure difference.

Pumps with overlapping geometry (Figure 6 (b) and (d)) are practically leakfree. Their volume flow, Q, is determined solely by the geometry and the rotational speed of the pump. The pressure difference, Δp, has almost no influence on Q.

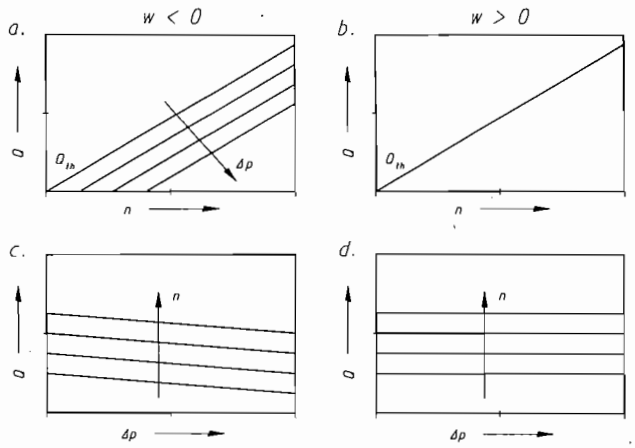

Figure 6. Flow Characteristics.

Power Consumption

The power input of the pump is determined by the effective hydraulic power, P_u, the load, P_S, due to internal slips and the losses, P_F, caused by the total of friction.

$$\begin{aligned} P &= P_{u,th} + P_F = P_u + P_S + P_F \\ &= Q_{th} \cdot \Delta p + P_F = Q \cdot \Delta p + S \cdot \Delta p + P_F \end{aligned} \tag{10}$$

The theoretical hydraulic power $P_{u,th}$ of the pump is defined by the geometry of the pump, the rotational speed and the pressure difference:

$$P_{u,th} = f\,(d_R, e, h_{St}, w, n, \Delta p) \tag{11}$$

The losses P_F due to friction are determined by the coefficient of friction μ of the rotor/stator materials and by the lubricating properties of the fluid:

$$P_F = f\,(\mu, \text{lubrication}) \tag{12}$$

The pump efficiency results from the energy balance of the pump as the ratio of effective power to total power consumption of the pump:

$$\eta_p = \frac{P_u}{P} = \frac{Q \cdot \Delta p}{Q \cdot \Delta p + P_F} = \eta_v \cdot \eta_m \tag{13}$$

This expression yields the basic power performance both for pumps with clearances (w < 0) and with overlapping (w > 0).

Pumps with clearance (Figure 7 (a) and (c)) demonstrate significant internal slip, S: the effective power, P_u, is noticeably lower than the theoretical power, $P_{u,th}$. The losses, P_F, due to friction, result mainly from fluid friction and are distinctly lower than those caused by mechanical friction of the displacement elements.

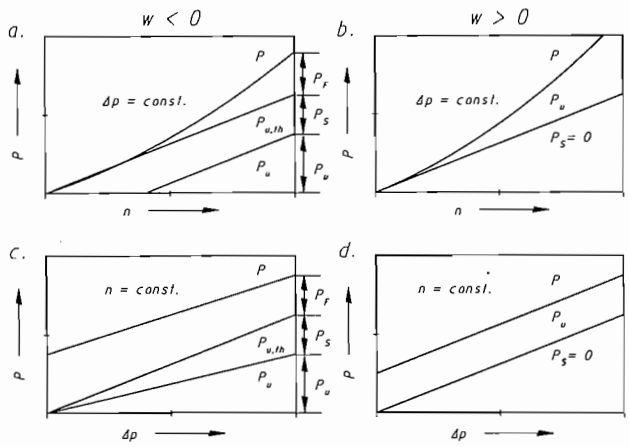

Figure 7. Power Characteristics.

Pumps with overlapping (Figure 7 (b) and (d)) feature negligibly low internal slip. Their effective power, P_u, is in good approximation determined by the theoretical power, $P_{u,th}$. The total power consumption, P, is additionally determined by the comparatively high losses, P_F, caused by friction between the displacing elements.

Operational Performance Tests

The characteristics determined experimentally and presented below are the result of exhaustive tests mainly performed with a standard pump permitting operation at high speed (Table 1).

Table 1. Data of the Pump Tested.

Industrial Pump NE 20B / 2 NQ 18	
Configuration	two stages
Housing	CrNi-steel 1.4301 welded
Rotor	CrNi-steel 1.4301
Stator	Ethylene-propylene-rubber, Shore A = 70
d_R	18 mm
e	3 mm
h_{St}	189 mm
Q	0 .. 5.6 m³/h
n	0 .. 3000 min⁻¹
Δp	0 .. 12 bar
P	0 .. 4.8 kW

Volume Flow

Since water was used in all tests, the internal slip losses are particularly recognizable. The volume flow, Q, shows an almost linear dependency on the speed n. As the transport pressure difference, Δp, increases, the flow deviates more and more from the geometrically determined volume flow, Q_{th}. The influence of the pressure differential on flow is much more pronounced in a pump with clearance (Figure 8 (a), w = - 0.15 mm) than in a pump with overlapping (Figure 8 b, w = 0.1 mm).

For a pump configuration with clearance and under the operational conditions selected, the influence of the pressure on the leakage flow is digressive, a remarkable observation. This response indicates a transition from laminar to turbulent flow through the clearance, where the leakage flow is correlated with the pressure differential via a square root relation. It clearly can be shown that under the respective conditions, the flow through the gaps is turbulent.

In pumps with positive overlapping, the dependency of the small internal slip due to the pressure differential is superimposed by the widening of the stator geometry by effects due to fulling of the stator related to the rotational speed of the pump.

The clearance, i.e., overlapping, w, clearly influences the hydraulic variables. (Figure 9). The volume flow, Q, for example, shows for a certain operating point (speed: 1000 min⁻¹, Δp: 5.0 bar) a distinct maximum (w = 0.1 mm). The decrease of the volume flow for growing w can be attributed to Equation (3). Of course, the slip, S, decreases as the clearance gets smaller. If the overlapping grows the slip stays approximately constant though fulling effects at the elastomer stator show certain influence.

Important remark: The slip flow statically measured at the blocked pump correlates well with the values determined as the pump operates. Apparently, for pumps with internal clearances, conclusions are admissible concerning the behavior during operation based on simple measurements of the leakage flow through the clearance while the transport elements are at rest. This relation is important and valuable, since in practice, due to the manufacturing tolerances present at the transport, elements the theoretical flow through the clearances cannot be evaluated with adequate accuracy.

Power

The required power, P, is increasing with speed and pressure differential. Surprisingly, the transition from a pump design with clearance (Figure 10 (a)) to one with overlapping geometry

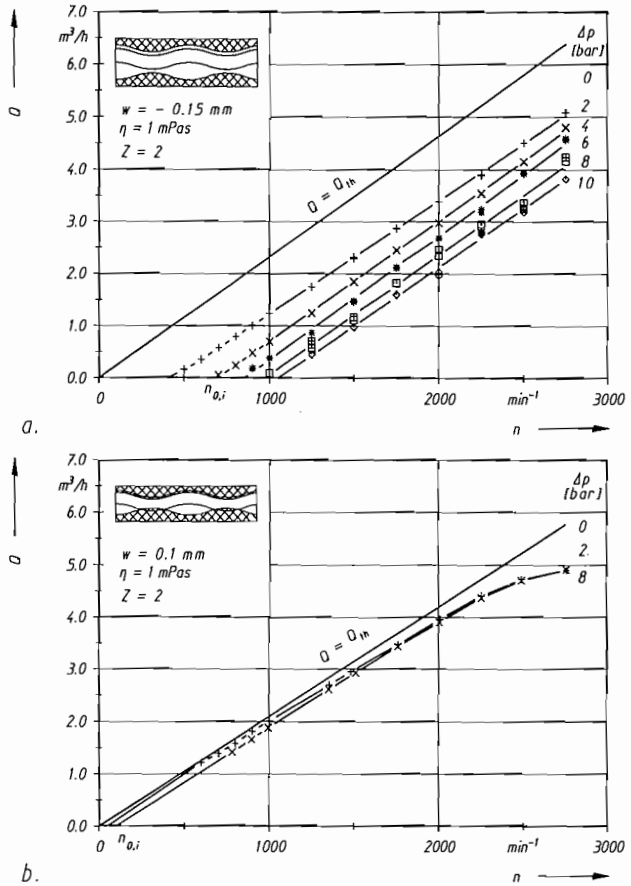

Figure 8. Flow Characteristics. (a) pump with clearances; and (b) pump with overlapping.

(Figure 10 (b)) results in a comparatively small increase in the drive power required.

The analysis of the individual components that influence the power required (Figure 11) makes this observation understandable.

As the w increases, the power losses due to slip (P_S) decrease and those due to friction (P_F) increase. Since the theoretical hydraulic power, $P_{u,th}$, declines slightly with w, on one hand an optimum of the effective, hydraulic power, P_u, is reached simultaneously while the required power P continuously increases.

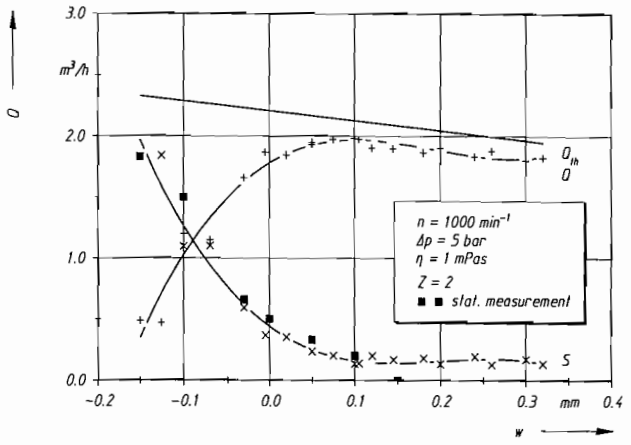

Figure 9. Flow, (Q), and Internal Slip, (S).

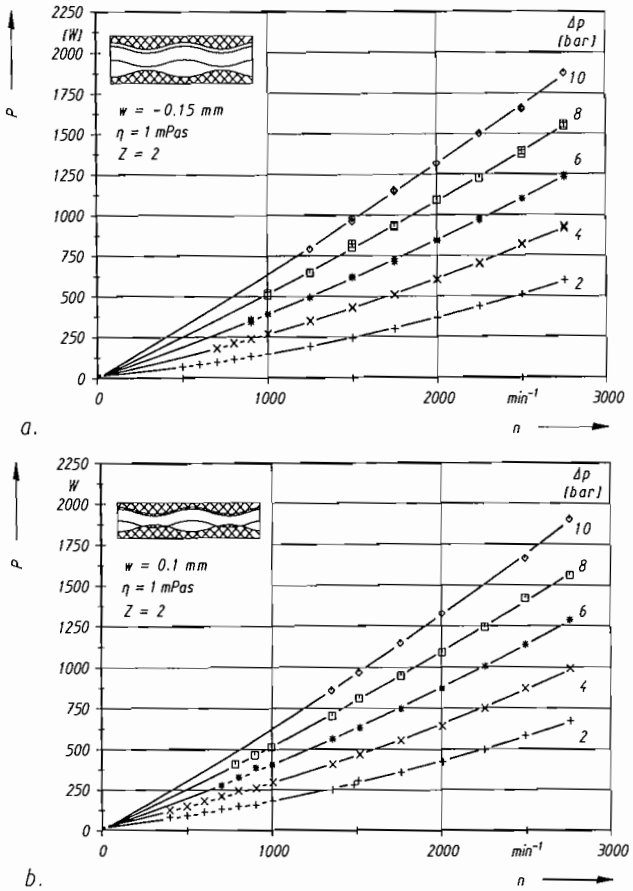

Figure 10. Power Characteristics. (a) pump with clearances; and (b) pump with overlapping.

Efficiency

The characteristics depicting the efficiency again demonstrate the opposed losses due to internal slip and friction (Table 2).

In pumps with clearance the volumetric efficiency, η_v, increases as the speed rises, since the internal slip flow stays approximately constant (Figure 12 (a)).

The mechanical efficiency, η_m, decreases as support forces if the stator and consequently friction losses increase. The pump efficiency η_P passes through a maximum (not yet reached in Figure 12 (a)), which shifts towards higher speeds as the differential pressure increases.

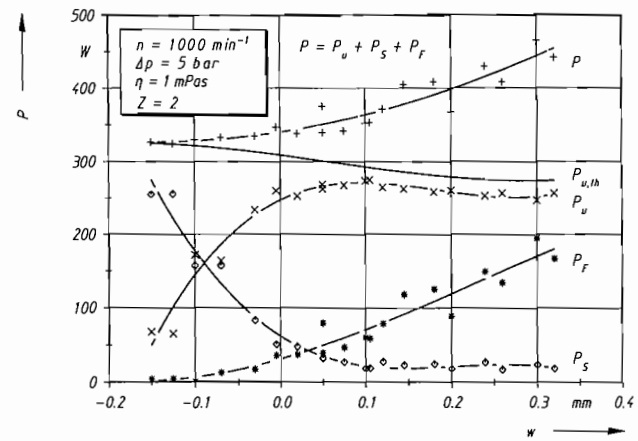

Figure 11. Balance of Power and Power Consumption, P.

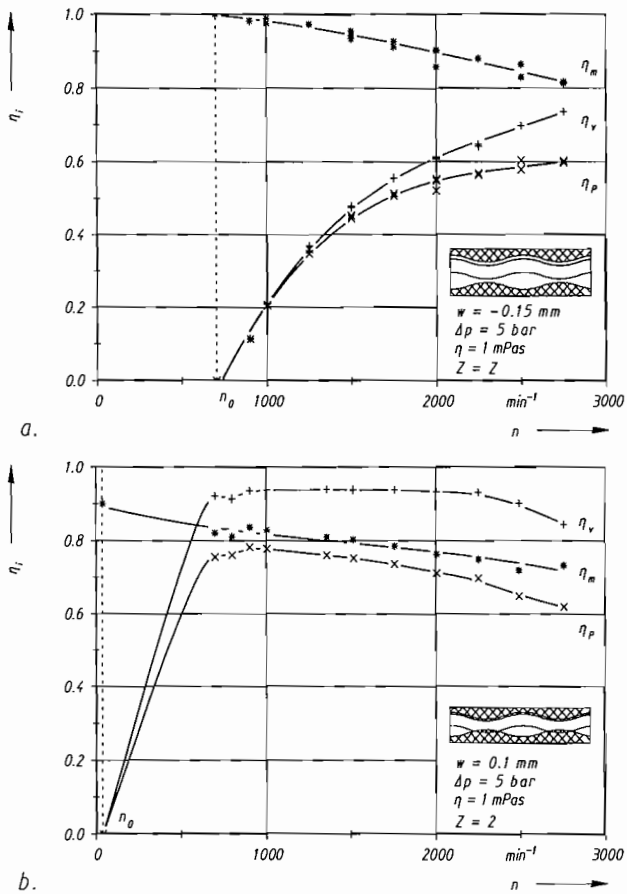

Figure 12. Pump Efficiency. (a) pump with clearances; and (b) pump with overlapping.

In pumps with overlapping (Figure 12 (b)) basically the same response can be observed. The volumetric efficiency reaches a flat maximum at distinctly lower speeds, however, and then decreases again slightly. This decrease can be attributed to elastic deformation of the geometry in the sealing clearances, due to the effects of filling.

The volumetric efficiency decreases with growing pressure differential according to Equation (9). The mechanical efficiency rises for increasing pressure, since due to the higher internal pressure, the width of the stator increases and, consequently, the friction losses decrease.

Pumps with clearance (Figure 13 (a)) show a narrow peak for the pump efficiency at a comparatively low differential pressure, while overlapping results in a comparatively wide range for maximum efficiency, with distinctly higher absolute values as in pumps with clearance (Figure 13 (b)).

Quite obviously, for specific operational conditions, an optimal overlapping, w_{opt}, exists with respect to favorable efficiencies (Figure 14).

Table 2. Characteristic Efficiency Data.

w	η_v	η_m
w < 0	20 - 80%	> 90%
w > 0	> 90 %	60 - 80%

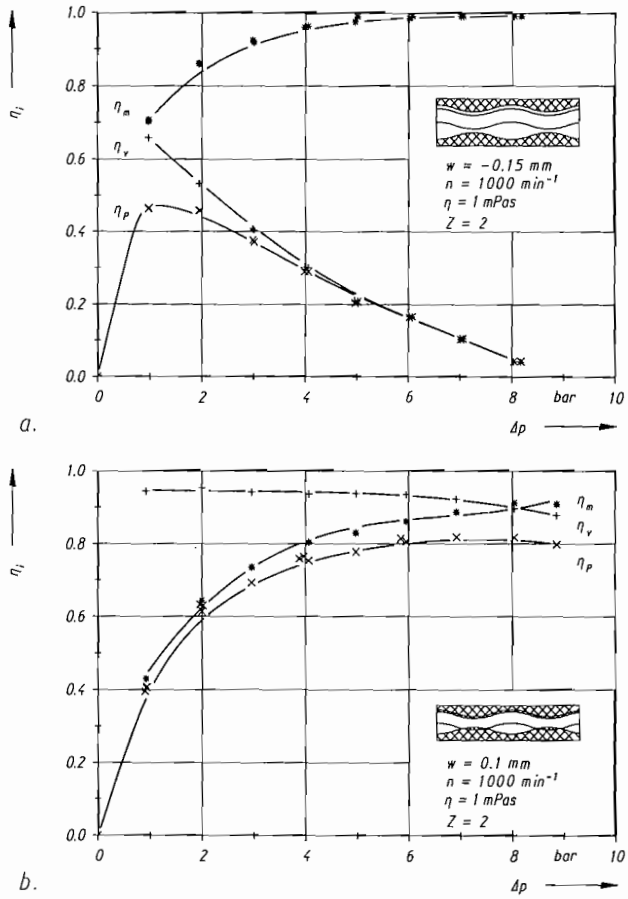

Figure 13. Pump Efficiency. (a) pump with clearances; and (b) pump with overlapping.

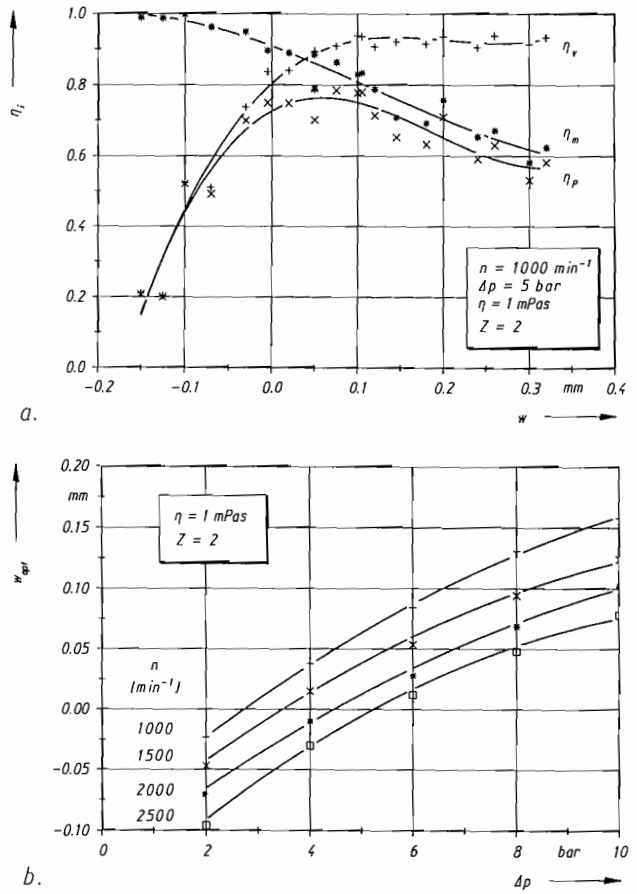

Figure 14. Optimal Overlapping. (a) optimum of efficiency, and (b) w_{opt}.

The decrease of the volumetric efficiency, η_v, for larger overlapping results on one hand from the decrease of the geometrically determined volume flow Q_{th} (Equation (3)), on the other hand from a change in the geometry and, accordingly, of the internal slip, S, due to fulling effects in the elastic elastomer stator.

The optimum of the pump efficiency, η_p, shifts by the way for rising pressure differential towards larger overlapping, w_{opt}.

Starting Torque

The characteristic of the starting torque constitutes a particular feature of the progressing cavity pump. To overcome static friction and depending on the degree of overlapping compression the starting torque, $T_{st,max}$, may typically be between two and four times as large as the operational torque, T_o.

$$f_T = \frac{T_{St,max}}{T_o} \qquad (14)$$

The amount of clearance, respectively, overlapping w (Figure 15) has a dominating influence on the starting torque, T_{St}. As the overlapping, w, increases, the starting torque increases dramatically. Depending on the lubricating properties of the fluid, a pump with clearance ($w < 0$) shows a typical starting factor f_T of 1.1, while overlapping features may result in starting factors up to $f_T = 4.1$. For typical operational conditions ($w = 0.1$ mm ; $\Delta p = 5$ bar) a starting factor $f_T = 2$ can be assumed.

This finding indicates a temporary absence of a lubricating film supporting low coefficients of friction, μ. This assumption can be verified with tribological investigations (ROS-tribometer). The influence of lubrication by the fluid on the coefficients of friction, μ, shows in Figure 16. Depending on the fluid viscosity, the range of mixed and fluid friction ($\mu < 0.1$) is characterized by a digressive or progressive course of the coefficients of friction with speed (Figure 16). Values for dry friction have also been entered into the diagram. As expected, the

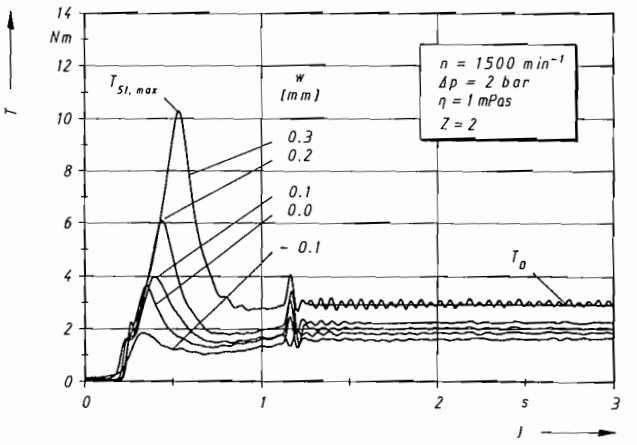

Figure 15. Starting Torque.

coefficients of friction are then approximately a magnitude higher and correlate with the coefficients of friction from startup tests (solid markers in Figure 16). The conclusion to expect a direct contact between the stator and the rotor of the pump during standstill appears to be reasonable.

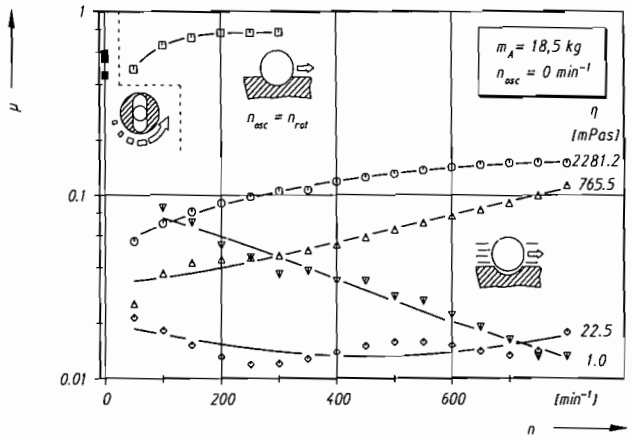

Figure 16. Coefficients of Friction.

Modelling Pump Efficiencies

Due to the poor definition of the clearances, a comprehensive mathematical description of the pump efficiency by computation of the internal slip, S, and the friction losses, P_F, cannot furnish a satisfactory result. Nevertheless, an approach for a theoretical estimation of the pump efficiencies based on preliminary tests will be presented.

The experimental investigations have clearly demonstrated the differences in the efficiencies characteristics for pumps with different clearances, respectively, overlapping.

- A pump with internal clearance (w < 0) shows noticeable internal slips but negligible friction, i.e., a moderate volumetric efficiency, η_v, but a good mechanical efficiency, η_m.
- A pump with overlapping is almost leakfree, the volumetric efficiency is close to 100 percent, but significant friction occurs.

From these conditions a strategy for estimates is derived:

- Pumps with clearance show a satisfactory correspondence of the slip measured statically and during operation of the pump (Figure 17). Static measurements, therefore, permit a reasonably accurate prediction of the volumetric efficiency, η_v. Assumption of a value of 90 to 95 percent for the mechanical efficiency, η_m, is acceptable.
- The slip of pumps with overlapping is small, which is well reflected by values of 90 to 95 percent for the volumetric efficiency. The friction losses can be determined with tribometer tests (Figure 16).

The results demonstrate good correlation of the experimentally determined operational losses, P_F, with increasing overlapping and theoretical modelling based on friction features from tribometric tests. The hypothesis of elevated internal temperature of the stator (T = 30°C in Figure 18) is confirmed. The modelled friction losses for a temperature T = 30°C clearly represent the measured values better.

ABRASIVE WEAR AND TRIBOMETRIC SIMULATION

Progressing cavity pumps are typically suitable for abrasive fluids like sewage, suspensions of TiO_2, or china clay slurries in the ceramics industry. Thanks to the combination of a hard rotor with an elastomer stator, the pumps offer superior service. The tribosystem of the pump, characterized by predominantly pushing transport of the particles and by elasticity and capability of the stator for imbedding of particles forms, the base for the favorable properties against abrasive wear (Table 3).

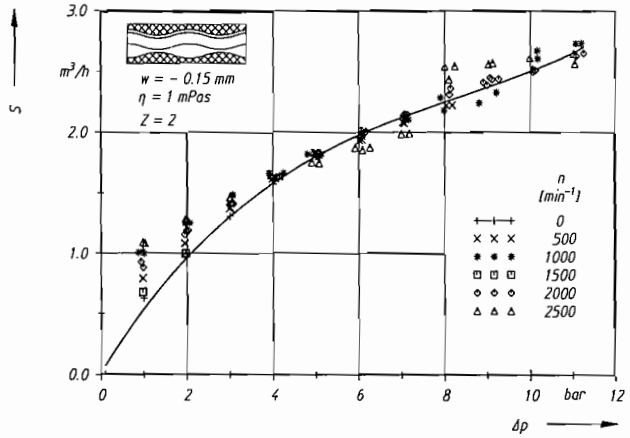

Figure 17. Leakflow at Statical and Dynamical Conditions.

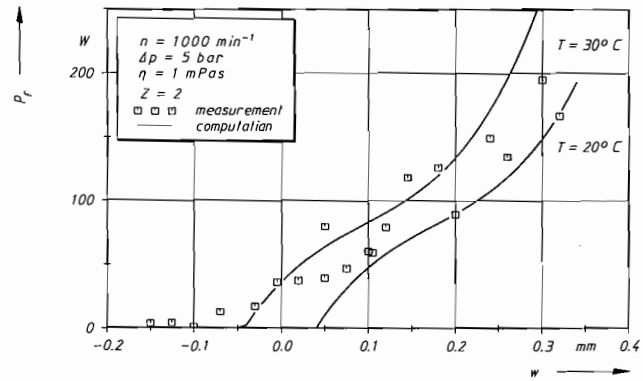

Figure 18. Modelling Friction Losses.

In spite of the inherent advantages in the face of abrasive attack, efforts to extend the operational life of the transport elements are essential, as long duty cycles are decisive for economical operation and reliability of the pump installation.

The Tribological System of Progressing Cavity Pumps

Sliding wear is predominating. It is determined by the relative motion of the displacement elements under pressure while the

Table 3. Parameters Influencing the Wear.

Variable	Effects abrasive wear
Hardness HV_M of the rotor material	--
Hardness Shore A of the stator elastomer	+
Hardness HV_P of the particles	++
Average grain size d_P	++
Concentration c_S of the particles	++
Time period of the operation	+
Contact compression $\bar{p}$	+
Sliding velocicty v_g	+
Corrosion (pH < 7)	+

fluid containing numerous particles is present in the zone of sliding (Figure 19).

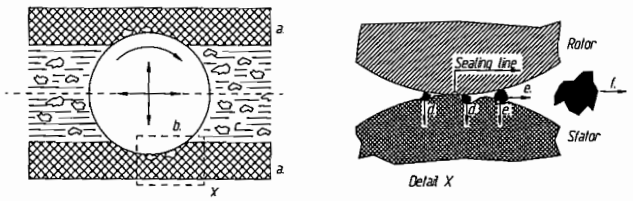

Figure 19. Tribological System. (a) elastomer stator; (b) rotor; (c) suspension; (d) imbedding; (e) transfer; and (f) rejection.

Based on the different hardness of the contact partners, and depending on the grain size, the particles are rejected (Figure 19 (f)), imbedded (Figure 19 (d)) or transferred in the sliding zone. Embedding decreases the sliding wear. Besides the dominating sliding wear, wear due to stamping motion and jetting wear in the sealing clearances occurs.

The process of wearing is also affected by the deformations of the elastomer of the stator by filling. Local changes in the geometry of the cavity of the stator affect the entering of particles into the sealing zone.

In practice, the abrasive wear of the pump manifests in a drop of the discharge flow of the pump. The internal clearances get wider, the slip, S, rises and reduces the effective volume flow, Q, according to Equation (5).

Meshing Situation

The process of wear in the pump is defined by the mutual meshing of the displacement elements. Investigations showed the wear not occurring uniformly on the entire outer surface of the rotor, but rather in a characteristic helical, ribbon shaped zone of wear (Figure 20). As compared with other areas, in this zone of the rotor extreme wear occurred. At both ends, the ribbon of wear fans out. With respect to the sense of rotation of the rotor, the ribbon of wear leads by approximately 30 degrees with respect to the vertex of the cross section of the rotor.

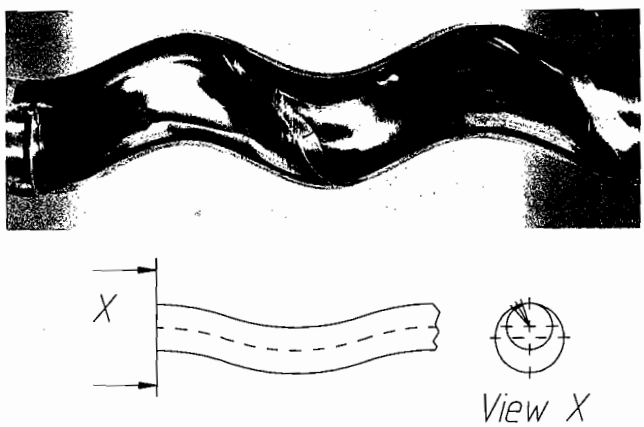

Figure 20. Sliding Wear at the Rotor of a Progressing Cavity Pump. (Field test: d_R = 60 mm, water/quartz-suspension, 2000 h.)

Evaluation of the traces of individual points at the circumference of the rotor depending on their position, δ, and the overlapping w yields a path of engagement, S_E, along which the particular point of the rotor is in contact with the stator during a full rotation of the rotor (Figure 21). The length of these paths of engagement, S_E, correlates excellently with the wear patterns measured on worn rotors (Figure 22).

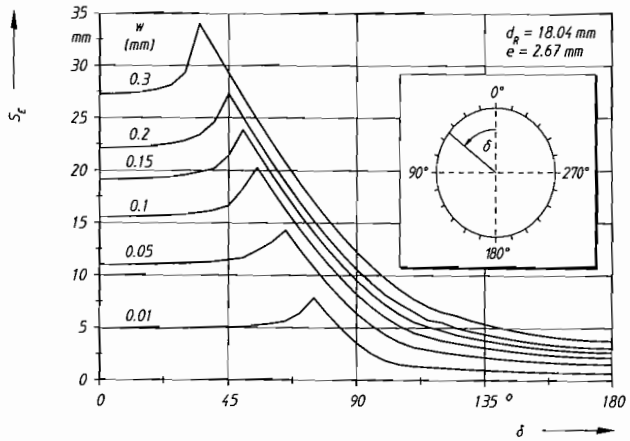

Figure 21. Meshing Situation.

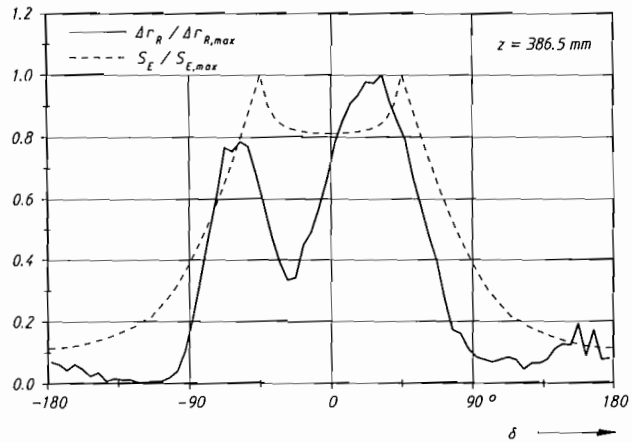

Figure 22. Meshing Situation and Rotor Shape Measurement.

Steps Towards Wear Reduction

Field tests with the pump are usually quite expensive. A simulation in a comparably simple tribometer is more economical. The tribosystem of the pump indicates the approach towards a simulation of the operation of the pump:

- The Miller-tribometer, well known from slurry technology, is suitable for qualitative investigation of materials for a specific problem [7].
- Simulation of the complex kinematics and meshing of the displacement elements is necessary for a quantitative determination and simulation of the response of the pump with respect to wear.

Basic investigations [6] with the Miller-tribometer and qualitative comparisons with the actual response of pumps show the fundamental influence of the parameters:

$$\Delta m = f\ (HV_M, \text{Shore A}, HV_p, d_p, c_s, t, \bar{p}, v_g, pH) \qquad (15)$$

During pumping of finely grained suspensions, the abrasive wear is predominantly determined by the ratio of the hardness of

the rotor material *vs* the hardness of the particles. Extensive data are available for the entire range of materials suitable for the rotor from austenitic chromium-nickel alloyed steels up to tungsten-carbides (hard metal types, HV_M = 200 .. 1500), allowing minimizing wear in the pump by the method of relative qualification. For the evaluation of fluids with unknown properties of the particle contents and the corrosion attack, execution of a Miller-test is sufficient to permit selection of the suitable materials. For several typical parameter influences such as the particle concentration, mean diameter of the particles and the hardness, simple correlations are available for conversion of wear rates (Table 4).

Table 4. Data of the Materials.

Identification code	Designation	Hardness
1.4301	X 5 Cr Ni 18 9	HV 160
1.2080	X 210 Cr 12	HV 215
1.2436	X 210 Cr W 12	HV 490 .. 781
CB	Poly-butadiene rubber	Shore A 60
SB	Nitrile rubber	Shore A 65 .. 70
VN	Polyurethane	Shore A 65 .. 92

As the mechanism by which the particles enter into the zone of wear differs in the Miller-tribometer from the actual conditions in the tribosystem of the progressing cavity pump, significant differences exist between the two systems.

For more precise simulation, the rotary oscillation sliding tribometer (ROS-tribometer) simulating the rotary and oscillatory motion of the rotor is used (Figure 23).

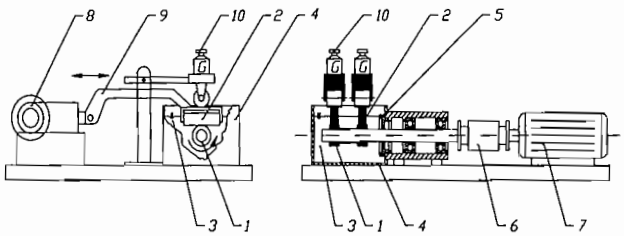

Figure 23. ROS-Tribometer. 1) metal sample; 2) elastomer sample; 3) test fluid; 4) fluid reservoir; 5) shaft seal; 6) torque meter; 7) rotary drive; 8) oscillating drive; 9) connection rod; and 10) weight deposited.

The sample of elastomer (2) is driven by the oscillating drive (8) via the connection rod (9) and performs a motion with harmonic characteristic crosswise to the sample of metal (1). The annular sample of metal is fastened on a shaft driven by the motor (7). The torque applied can be measured between the drive and the bearing with an electronic torquemeter (6). The compression between the sample elements can be simulated by means of the weight (10).

The ROS-tribometer described in detail by Wirth [6] permits determination of all relevant data of the pump and furnishes quantitative information on the actual wear mechanism. It allows the testing of more than on pair of samples (Figure 23 shows two of them) at a time with continuous agitation of the suspension.

The mode of entering of the particles and the meshing conditions in the ROS-tribometer differs somewhat from the situation in progressing cavity pumps, a fact which has to be mentioned expressively. For the simulation of a specific tribological case, transfer factors have to be used, therefore, which have been investigated more closely [6]. Correlations open for calibration exist for example between the weight deposited, the geometry of the samples and the overlapping geometry in the pump.

Results from ROS-Tribometer Tests

Investigations with the ROS-tribometer represent a good approach to achieve extended service life of the pump for the various parameters. The results quoted below are a small excerpt dealing with specific tribosystems (quartz sand with a specific particle size distribution suspended in water). The respective data such as the mean particle size, d_p, the concentration, c_s, of solids, the pH-value and the combination of materials used in the test (e.g., 1.4301 / SB) are given in the applicable places.

For the ROS-tribometer, commonly the same frequency is selected for the rotation and the oscillation (n_{osc}/n_r = 1), meeting the real conditions in the pump.

(The expression n_{osc}/n_r = 100/100 means: both frequencies = 100 min^{-1}).

Influence of the Contact Compression

The overlapping in the pump and the contact compression in the ROS-tribometer are directly related. The influence of the contact compression is approximately linear. In a ROS-tribometer the area of contact increases as the compression rises, while the area of contact stays constant in the Miller-tribometer (Figure 24).

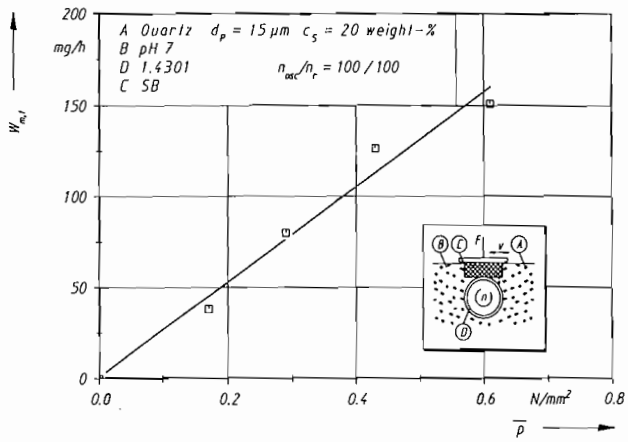

Figure 24. Influence of Contact Compression on the Wear Rate, $W_{m.t}$

Influence of the Speed

The difference between purely rotational motion (n_{osc}/n_r = 0) and simultaneous rotation and oscillation of the sample, both at the same frequency (n_{osc}/n_r = 1) manifests almost dramatically. The gradient for the rate of wear during rotational motion only decreases as the speed rises, since a film of lubricant capable of supporting the surfaces involved develops and the particles are partly rejected (Figure 25).

During simulation corresponding to the actual conditions (n_{osc}/n_r = 1), the wear increases approximately linearly with the rotational speed however. In this mode of operation, new particles continue to enter the zone of engagement between the two displacement elements and the formation of a film of lubricant is obstructed.

Data useful for a prognosis for the service life of the pump can, therefore, be collected via tribosimulation duplicating the actual kinematics present in the pump. These findings confirm the expectation that a quantitative simulation of the progressing

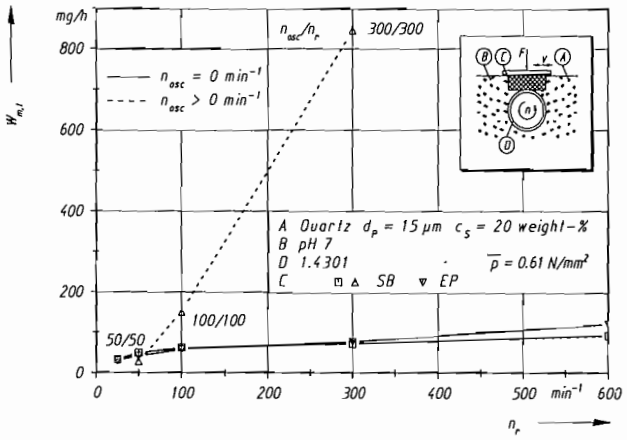

Figure 25. Influence of Speed on the Wear Rate, $W_{m,t}$ (Sample diameter = 75 mm).

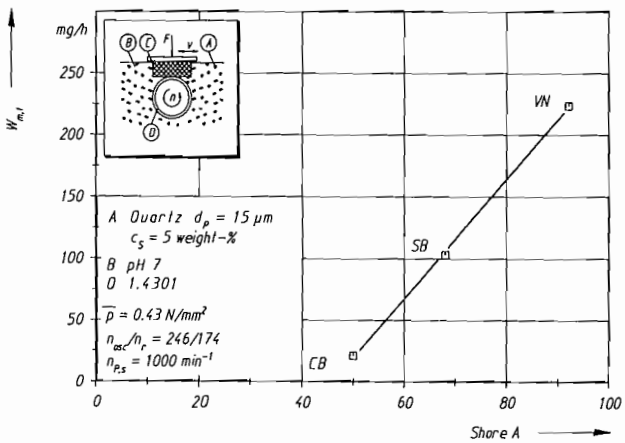

Figure 27. Influence of the Elastomer Hardness on the Wear Rate, $W_{m,t}$.

cavity pump by means of the Miller-tribometer (oscillatory motion of the sample only, no rotational motion) is impossible.

Influence of the Rotor Hardness

To suppress any eventual influences of corrosion the investigations were conducted at a pH = 12. The results (Figure 26) correspond qualitatively with the known characteristics obtained via the Miller-tribometer [8] and the data collected during operational testing [6].

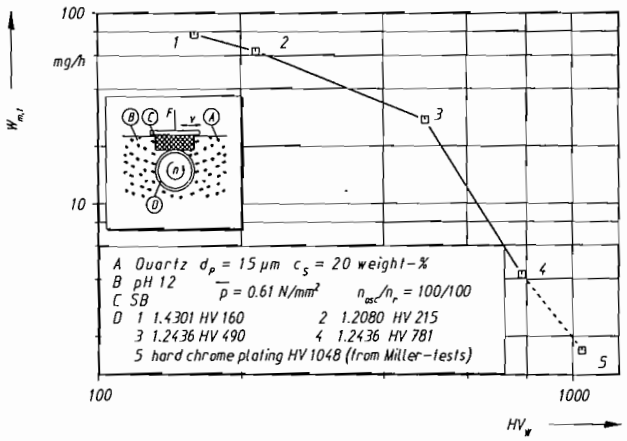

Figure 26. Influence of the Hardness of the Rotor Material on the Wear Rate, $W_{m,t}$.

In plots with a logarithmic scale in some sections a linear dependence of the wear rate on the hardness of the material can be noted. For a transition from soft chromium-nickel steel 1.4301 (HV 160) to a hardened chromium-alloyed steel 1.2436 (HV 781), the wear rate drops, for example, by a factor of 20! For an even harder material (hard chrome plating) this factor rises approximately to 40. Under these conditions, the tribosystem arrives at the minimum wear position as particle and material hardness demonstrate the same magnitude (Hardness of quartz: HV approximately 1200).

The service life can, therefore, be extended most effectively via the hardness of the material of the rotor (Figure 27).

Like the Miller-tribometer, the ROS-tribometer allows statements concerning the relative suitability of materials to solve a specific wear problem.

Influence of the Elastomer Hardness

In the hardness range between 50 and 80 shore, the rate of wear rises approximately linearly as the hardness of the elastomer samples increases.

Lesser hardness results in deeper imbedding of the solid particles into the elastomer and, so, to a lower rate of wear.

These results correlate well with the results obtained in the Miller-tests.

Influence of the Concentration of Solids

An increasing concentration of solids in the suspension results also in the ROS-tribometer in rising wear rates, which increase additionally with rising speed. More solids may reach the area of engagement under these conditions.

In the ROS-tribometer as well as in the Miller-tribometer the rate of wear does not rise substantially any more for concentrations of solids exceeding approximately five to ten percent by weight. This typical phenomenon can be attributed to the rejection of the particles causing wear from the zone of engagement for higher concentrations of solids.

Service Life Tests with Progressing Cavity Pumps

The investigations conducted with a ROS-tribometer show the following parameters for optimization of the pump under abrasive wear:

- less overlapping w (lower contact compression)
- lower rotational speed n
- higher hardness HV_M of the rotor material
- lower hardness Shore A of the elastomer

The service life, t_L, of a pump is defined as the period of time until the pump during a specific conveying task (Δp, η, c_S, HV_P, HV_M) delivers a certain minimal volume flow Q_{min}.

The range of potential for optimization of the pump can, for example, be shown for a variation of the hardness, HV_M, of the material used for the rotor. The wear rate is shown in Figure 28 of pump rotors made of different materials pumping a suspension of quartz sand in water. The lower relative wear of harder materials for the rotor is distinctly recognizable. The gradual decline of the discharge flow for the sample pump with respect

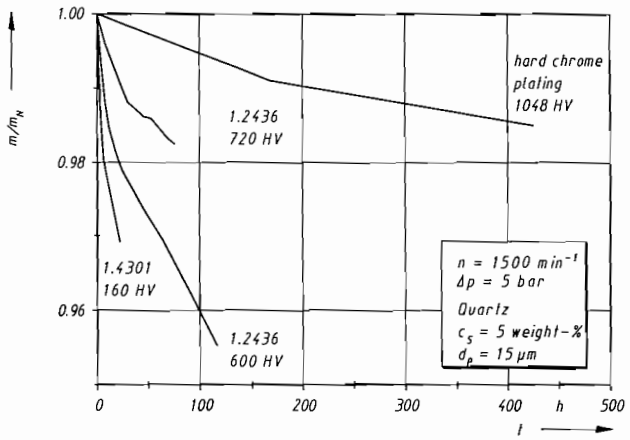

Figure 28. Wear Rate of the Pump Rotor.

to time is explained in Figure 29, the Q_{min}-line marking the minimum acceptable discharge. The intersection of the characteristic, Q(t) with Q_{min} = constant, yields the individual service life, t_L.

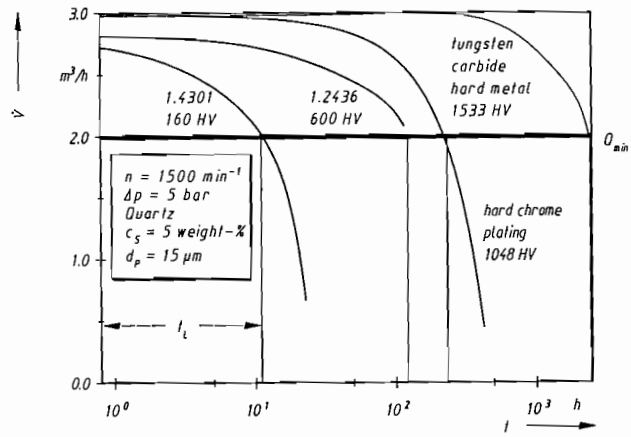

Figure 29. Delivery Characteristics.

The pump fitted with a hard chromium plated rotor has approximately 25 times the service life of a pump with a rotor made of stainless steel 1.4301. The characteristic for the service life of a pump with a rotor made of a tungsten carbide hard metal is based on estimates, demonstrates 250 times longer endurance compared to a stainless steel (1.4301) rotor. All these field test results can be predicted fairly well by tribometer tests (ROS-tribometer).

Simple investigations using tribometers accordingly permit the determination of wear parameters and to develop a sequence of materials corresponding to increasingly longer service life of the pump. These data allow at least a qualitative prognosis for the amount of wear to be expected, and, consequently, a reasonable forecast concerning the expectable service life of the pump.

A quantitative prognosis concerning wear and, therefore, a reliable estimate for the service life of a pump in a specific application is already feasible in isolated cases [6], but requires more knowledge about the tribological system involved on tribometric and on the pump side.

With progressing cavity pumps, the challenge of quantitative life time prognosis involves the analysis of the contact compression during pump operation. As a matter of fact, quantitative wear prediction actually is only feasible for a pump with overlapping geometry.

CONCLUSIONS

The progressing cavity pump represents a widely used type of pump predominantly used for the transport of nonlubricating, abrasive or highly viscous fluids. This study was intended to investigate the parameters influencing the basic performance and to contribute towards understanding of the typical characteristics of this type of pump. The process of abrasive wear in the pump had to be simulated in a suitable tribometer to determine the influences of the operational parameters. These data were expected to yield options and potentials for optimization of the pump, to allow prolongation of the service life of the pump, based on the operating conditions.

The investigations concerning the discharge flow, with respect to the pressure differential and the speed, prove the progressing cavity pump to exhibit the typical linear, rather pressure stiff characteristics of a displacing machine. The clearance, i.e., the overlapping, has a decisive influence on discharge flow and efficiency. For a given pressure differential, an amount of overlapping, w_{opt}, yielding optimal pump efficiency can be determined.

The insights obtained permit a preliminary performance estimate based on simple initial investigations on the static slip of the pump and the coefficients of friction by a tribometric approach. The values collected this way can be applied towards the dynamic operation of the real pump with satisfactory accuracy.

Abrasive wear in the presence of particles in the sliding zone in the progressing cavity pump is predominantly determined by sliding friction. A sliding type tribometer capable of duplicating the special kinematics of the displacement elements in a range of the contact velocity relevant to the operational circumstances permits a tribometric simulation. This ROS-tribometer allows the tribometric simulation of the conditions in a pump operating with nominally overlapping geometry.

The parameter influences with the ROS-tribometer are clearly demonstrated. As a matter of fact, the ROS-tribometer meets the quality of simulation much better than the Miller-tribometer, both methods being very applicable for qualitative information about the relative suitability of materials.

The results of such a tribometric simulation permit a prolongation of the service life of the progressing cavity pump via intentional variation and selection of the properties of the materials and the operational conditions determining the wear. This is verified in a number of field tests with quartz-suspensions and rotor materials varying from austenitic stainless steel to tungsten-carbide hard metals, extending the service life time by a factor of 250.

NOMENCLATURE

Symbol	*Unit*	*Designation*
δ	degree	angular position
η	Pas	dynamic viscosity
η_i	-	efficiency
η_P	-	pump efficiency
η_m	-	mechanical efficiency
η_v	-	volumetric efficiency
μ	-	coefficient of friction
φ	degree	angle of rotation
c_s	kg/m³	concentration of the slurry
D	m³	displacement volume
d_p	mm	diameter of the particle

d_R	mm	diameter of the rotor
d_{Ring}	mm	diameter of the sample of metal of the ROS-tribometer
d_{St}	mm	diameter of the stator
e	mm	eccentricity
F	N	force
h_R	mm	pitch of the rotor
h_{St}	mm	pitch of the stator
HV_p	-	Vickers hardness of the wear particles
HV_M	-	Vickers hardness of the base material
m	kg	mass of the rotor
m_A	kg	weight on the ROS-tribometer
m_N	kg	mass of the rotor preceding the wear test
n	min^{-1}	rotational speed
n_0	min^{-1}	pump speed at starting delivery
n_{osc}	min^{-1}	stroke frequency of the oscillatory drive of the ROS-tribometer
n_r	min^{-1}	speed of the rotational drive of the ROS-tribometer
$n_{s,P}$	min^{-1}	pump speed simulated by the ROS-tribometer
$\bar{p}$	N/mm^2	contact compression
P	W	input power
P_u	W	effective hydraulic power
P_S	W	hydraulic slip power
$P_{u,th}$	W	theoretical hydraulic power
pH	-	pH-value
P_F	W	power losses due to friction
Δp	bar	pressure difference
Q	m^3/h	volume flow
Q_{min}	m^3/h	volume flow at the end of the service life
Q_{th}	m^3/h	theoretical volume flow
Δr_R	mm	wear on the rotor
S	m^3/h	slip
S, lam	m^3/h	laminar slip
S, turb	m^3/h	turbulent slip
S_E	mm	path of engagement
s	mm	gap width
t_L	h	service life
T	°	temperature
T_o	Nm	operational torque
t	s	time
T_{St}	Nm	start-up torque
v	m/s	velocity
v_g	m/s	velocity of sliding
w	mm	rated clearance, resp. overlapping
$W_{m,t}$	mg/h	rate of loss of mass
w_{opt}	mm	clearance, resp. positive interference corresponding to the optimal pump efficiency
Z	-	number of stages

REFERENCES

1. Vetter, G. and Wirth, W., "Suitability of Eccentric Helical Pumps for Turbid Water Deep Well Pumping in Photovoltaic Systems," Solar Energy 51 (3), No. 3, pp. 205-214 (1993).
2. Vetter, G. and Wirth, W., "Wirkungsgrad- und Verschleißuntersuchungen an Exzenterschneckenpumpen im Hinblick auf ihre Anwendung in photovoltaischen Wasserförderungsanlagen," Photovoltaische Energieversorgung für Geräte im kleinen und mittleren Leistungsbereich, Abschlußbericht des Forschungsvorhabens 0328689A des BMFT, Hrsg. Schmid, J. et al. (1991).
3. "Firmenschrift 1.3000.005," Bornemann GmbH & Co. KG, Obernkirchen.
4. "Firmenschrift NM 009/01," Netzsch Mohnopumpen GmbH, Waldkraiburg.
5. "Firmenschrift VM 6.368/10.83," VM586/2.85, Allweiler AG, Radolfzell
6. Wirth, W., "Zur hydraulischen und tribometrischen Simulation von Exzenterschneckenpumpen," Dissertation, Universität Erlangen-Nürnberg (1993).
7. "ASTMG 2.3, Standard Test Method for Slurry Abrasivity Determination," 11-16-80 (1980).
8. Vetter, G., Klotzbücher, G., "Einige tribologische Grundlagenuntersuchungen zum abrasiven Gleit- und Strahlverschleiß von Pumpenwerkstoffen," Konstruktion, 45, (1993), pp. 371-378 (1993).
9. "Operating Manual, The Miller Machine," White Rock Engineering, Dallas, Texas (1986).